NANO: Brief Reports and Reviews
Vol. 15, No. 5 (2020) 2050059 (10 pages)

DOI: 10.1142/S1793292020500599

Three-Dimensional Graphene Oxide-Supported Zinc Oxide Scaffold as a High-Efficiency Adsorbent for Desulfurization

Yan Liu*, Xiaojun Zhang†, Meiyan Yang†, Bowen Guo†,§,**, Jixiang Guo‡,¶,** and Dan Luo†,‖,**

*Laboratory of Biomimetic Nanomaterials
Department of Orthodontics
Peking University School and Hospital of Stomatology
Beijing 100081, P. R. China

†State Key Laboratory of Heavy Oil Processing
College of New Energy and Materials
Beijing Key Laboratory of Biogas Upgrading Utilization
China University of Petroleum (Beijing)
Beijing 102249, P. R. China

‡The Unconventional Petroleum Research Institute
China University of Petroleum (Beijing)
Beijing 102249, P. R. China
§bowen0321@163.com
¶guojx002@163.com
‖luodan@cup.edu.cn

Received 1 December 2019
Accepted 6 March 2020
Published 22 May 2020

Sulfur oxides are air pollutants derived mainly from the combustion of gasoline. Reducing the sulfur content of fluid catalytic cracking (FCC) gasoline is of key importance for the prevention and control of atmospheric pollution. We describe herein the fabrication and characterization of a porous, three-dimensional (3D) graphene oxide-supported zinc oxide (GO/ZnO) scaffold as an adsorbent for desulfurization with various model compounds and real FCC gasoline. The uniform and stable dispersion of ZnO nanoparticles on the surface of GO facilitates the specific binding of sulfides. Moreover, GO synergistically adsorbs aryl sulfides via π–π stacking interactions. The GO/ZnO nanosheets were further self-assembled into a 3D porous scaffold that effectively trapped sulfides and inhibited desorption. These scaffolds exhibited excellent desulfurization performance with maximum sulfur capacity up to 29.73 mg S/g. This work provides a novel perspective on the fabrication of high-efficiency adsorbents for gasoline pretreatment.

Keywords: Graphene oxide; ZnO; nanocomposite; adsorption desulfurization.

**Corresponding authors.

1. Introduction

Sulfur oxides produced by the combustion of sulfur-containing transportation fuels are atmospheric pollutants that can ultimately result in sulfuric acid mist and acid rain. To prevent such pollution, the international community is paying considerable attention to atmospheric governance; one strategy involves controlling sulfide levels in gasoline. The Chinese National VI emission standard stipulates that the total sulfur content of gasoline must not exceed 10 mg/kg. Ultra-deep desulfurization technologies, including hydro-, adsorption, oxidative, and extraction desulfurization processes, have shown effectiveness for removing sulfides from gasoline.[1–6] However, hydrodesulfurization requires high temperatures and pressures that ultimately reduce the octane rating of gasoline and cannot efficiently remove refractory sulfur compounds such as benzothiophene (BT).[7–10] Catalytic oxidative desulfurization systems are toxic and expensive; the added oxidant can result in undesirable side reactions and the conversion of thiophene remains difficult.[11–13] Extraction desulfurization processes have poor sulfur removal rates ($<50\%$) with high co-extraction.[14] Of the available technologies, adsorption desulfurization is the most effective and straightforward method for removing sulfide contaminants from gasoline.

Zinc oxide (ZnO) is a common semiconductor material used widely as an adsorbent, corrosion protectant and catalyst due to its safety, stability and low cost.[15–19] ZnO possesses high chemisorption capacity, multi-layer adsorption characteristics and favorable thermodynamic properties for sulfidation,[15,20] making it one of the most widely used adsorbents for desulfurization. The relatively small surface area and low surface energy of conventional bulk ZnO adsorbents limit the thermodynamics and kinetics of sulfide adsorption. Reducing the dimensions of ZnO is of key importance for obtaining high adsorption desulfurization performance.[21] ZnO nanoparticles are promising as a desulfurization sorbent material because their quantum size effects could compensate for slow sulfidation kinetics. However, such nano-adsorption systems are typically unstable because their high surface energies can result in particle aggregation and, consequently, inactivation. Small-scale, dispersive, and stable nanosystems for desulfurization remain elusive.

Nanocarrier-based loading is an effective strategy to achieve uniform and stable dispersions of nano-adsorbent. The selection of carrier should meet the following characteristics: (i) a large surface area for nanoparticle loading, (ii) abundant exposed functional groups able to coordinate with the active component, and (iii) synergistic adsorption effects when combined with nanoparticles. Graphene oxide (GO) is an ideal two-dimensional (2D) carrier with a high theoretical specific surface area and rich, oxygen-containing functional groups. Moreover, the sp^2 domains of GO facilitate the binding of aryl and unsaturated heterocyclic compounds via π–π interactions.[22–25] We describe herein the fabrication of GO-supported ZnO nanoparticles (GO/ZnO) as a new generation of nanoadsorbents for the removal of sulfides from gasoline. Stable dispersions of ZnO nanoparticles on the surface of GO were shown to specifically bind sulfides.[26] In addition, the GO allowed for the adsorption of aryl sulfides through π–π interactions. To limit the desorption of sulfides, the GO/ZnO nanosheets were further assembled into three-dimensional (3D) porous structure to "trap" adsorbates. The resulting 3D GO/ZnO scaffolds were excellent adsorbents and exhibited high levels of desulfurization when applied to liquid fuels.

2. Experimental

2.1. *Synthesis of GO nanosheets*

GO was synthesized as follows: 0.75 g of graphite powder was mixed with 4.5 g of potassium permanganate to form a uniform powder; this was slowly added to a mixture of concentrated sulfuric acid and concentrated phosphoric acid (9 mL/1 mL), and stirred in a water bath at 50°C for 12 h. After the reaction was complete, the mixture was allowed to cool to room temperature and 100 mL of an ice-water mixture was added. A hydrogen peroxide solution was then added dropwise until the mixture turned bright yellow. At this point, the mixture was washed with 30% hydrochloric acid and deionized water at least three times to delaminate the GO and form single-layer sheets. The mixture was then centrifuged at 10 000 rpm for 30 min and the resulting pellet was washed and lyophilized.

2.2. *Synthesis of GO/ZnO nanocomposites*

GO/ZnO nanocomposites were prepared as follows: 30 mg of GO powder was dispersed in 75 mL of ethylene glycol to form solution A, and 0.5 mmol of zinc acetate was dissolved in 25 mL of ethylene glycol to form solution B as a metal precursor. Solutions A and B were combined and stirred for 60 min. The mixed suspension was then refluxed at 170°C for 2 h. The solution was then allowed to cool naturally to room temperature and washed with ethanol at least three times. The resulting product was dried overnight under vacuum at 150°C.

2.3. *Self-assembly into 3D GO/ZnO scaffolds*

Three-dimensional GO/ZnO nanocomposites were prepared from conventional GO/ZnO nanocomposites, as follows. GO/ZnO nanocomposites were repeatedly filtered and washed with deionized water to obtain a black GO/ZnO powder, which was then heated to 200°C and held at this temperature for 1 h in an Ar atmosphere to obtain the 3D GO/ZnO nanocomposites.

2.4. *Characterization*

Powder X-ray diffraction (XRD) diffractograms were obtained using a Rigaku D/MAX-2000 diffractometer (Rigaku Corporation, Japan) using Cu-Kα radiation ($\lambda = 1.5406$ Å). Field emission gun-transmission electron microscopy (FEG-TEM) was performed using a Philips Tecnai F20 instrument (FEI Company, USA) operated at 200 kV. Scanning electron microscopy (SEM) was performed using a Quanta200F instrument (FEI Company) with a resolution of 1.2 nm. Fourier-transform infrared spectroscopy (FT-IR) was performed with a VERTEX 70 instrument (Bruker Company, Germany) over a scanning range of 500–4000 cm^{-1} at a resolution of 8 cm^{-1}. Raman spectra were acquired using a LabRAM HR Evolution instrument (HORIBA Scientific, France). The sulfur contents of oils before and after adsorption were determined using an RPP-2000S ultraviolet fluorescence sulfur analyzer (Taizhou Zhonghuan Analysis Instrument Co., Ltd., China).

2.5. *Representative procedure for adsorption desulfurization*

In this experiment, dodecane was used as the solvent, ethyl mercaptan, diethyl thioether, thiophene and benzothiophene were used as typical sulfur-containing compounds to become the solute, and the petrol-like model compounds were configured with a certain concentration. Taking thiophene as an example, the sulfur content is calculated according to the following formula:

$$\frac{m_{\text{thiophene}}}{m_{\text{dodecane}} + m_{\text{thiophene}}} \times \frac{32.07}{84.14} \times 10^6. \qquad (1)$$

In a typical sorption procedure, 15 mg sorbent and a model compound (5 mL) were sealed in a high-pressure microreactor and the mixture was then heated at 200°C for 2 h. The sulfur adsorption capacity (normalized per adsorbent weight) was calculated based on the following equation[27]:

$$S = ((C_0 - C_t) \times \rho \times V)/m \times 10^{-3}, \qquad (2)$$

where S is the mass of sulfur adsorbed per gram of adsorbent (mg of S/g), C_0 is the initial sulfur concentration in the model fuel (mg/g), C_t is the sulfur concentration in the effluent (mg/g) at time t, ρ is the density of the model fuel (g/mL, e.g., the density of dodecane is 0.753 g/mL), V is the reaction volume of the model fuel (mL), and m is the mass (g) of the catalyst in the reaction.

The regeneration of catalysts was achieved after heating the used adsorbent at 350°C for 1 h under N_2 atmosphere.

3. Results and Discussion

3.1. *Characterization of the 3D GO/ZnO scaffolds*

The synthesis of 3D GO/ZnO porous scaffolds involved four steps: (i) fabrication of GO using an improved Hummers' method,[28–30] (ii) coordination between the functional groups of GO and Zn ions, (iii) *in situ* growth of ZnO nanoparticles on the surface of GO, and (iv) self-assembly of GO/ZnO into a 3D scaffold.[31] A schematic of this process is shown in Fig. 1.

The morphology of the obtained GO nanosheets was observed by TEM. Figure 2(a) shows that large-area, flexible, and silk-like GO was obtained with lateral dimensions of 5–10 μm.[32] Note that the

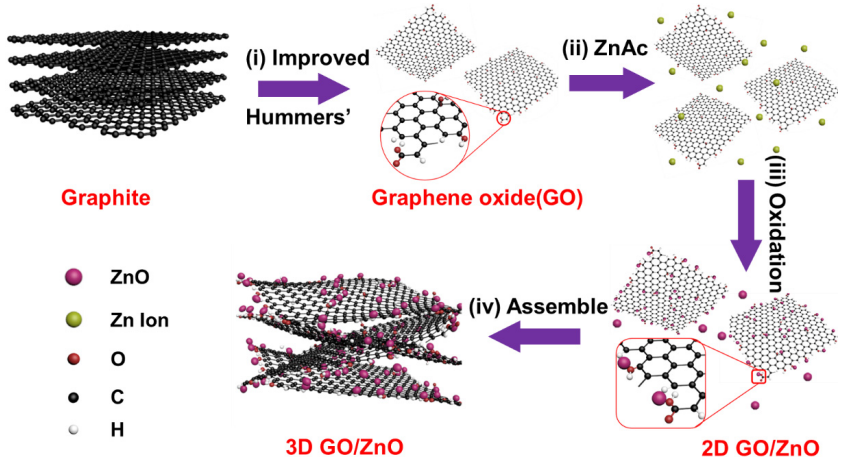

Fig. 1. Schematic illustration of the fabrication of 3D GO/ZnO porous scaffolds.

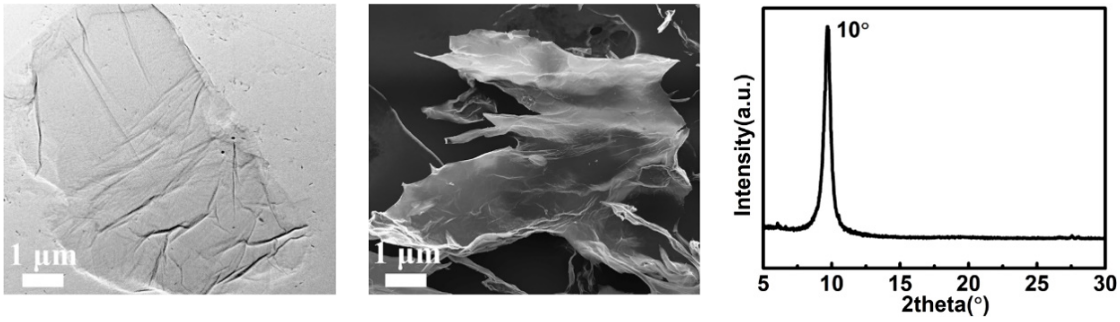

(a) (b) (c)

Fig. 2. (a) TEM, (b) SEM micrographs and (c) a powder XRD diffractogram, of GO.

GO nanosheets were symmetrical and thin, without obvious aggregation. The slightly wrinkled texture on the surface of GO can be ascribed to distortions caused by carbon atoms bound to hydroxyl groups in a tetrahedral structure. The SEM micrographs in Fig. 2(b) show high-quality, ultrathin GO nanosheets with large surface areas. The XRD diffractograms in Fig. 2(c) contain a strong diffraction peak at around 10°, corresponding to the (001) plane of GO. There is no diffraction peak corresponding to graphite. The interlaminar distance and overall quality of GO sheets increases with increasing oxidation. The XRD data in Fig. 2(c) indicate an interlayer spacing of 9.1 Å, which is significantly larger than that of graphite and can be attributed to the perturbation of oxygen groups bound to the graphite sheet.[33,34] These results further confirm the high quality of the obtained GO sheets.

The acquired GO nanosheets were then coordinated with zinc ions; further oxidation resulted in the in situ growth of ZnO nanoparticles, forming GO/ZnO nanocomposites. Note that the coordination of ions and subsequent growth of nanoparticles did not alter the morphology of the GO sheets. The TEM micrographs in Fig. 3(a) show large, 2D nanosheets of GO/ZnO with no obvious nanoparticle aggregation, similar in appearance to GO. The elemental distribution of GO/ZnO nanosheets was confirmed by scanning transmission electron microscopy coupled with energy-dispersive X-ray spectroscopy (STEM-EDS) mapping [Fig. 3(b)].

The results showed that zinc and oxygen were uniformly distributed on the carbon substrate. This indicates that the abundant functional groups of GO were effective in anchoring metal ions, resulting in a homogeneous distribution of adsorbent. The growth of ZnO was evaluated by high-resolution transmission electron microscopy (HRTEM). ZnO was evaluated by HRTEM. The resulting micrographs in Fig. 3(c) show ZnO nanoparticles with an

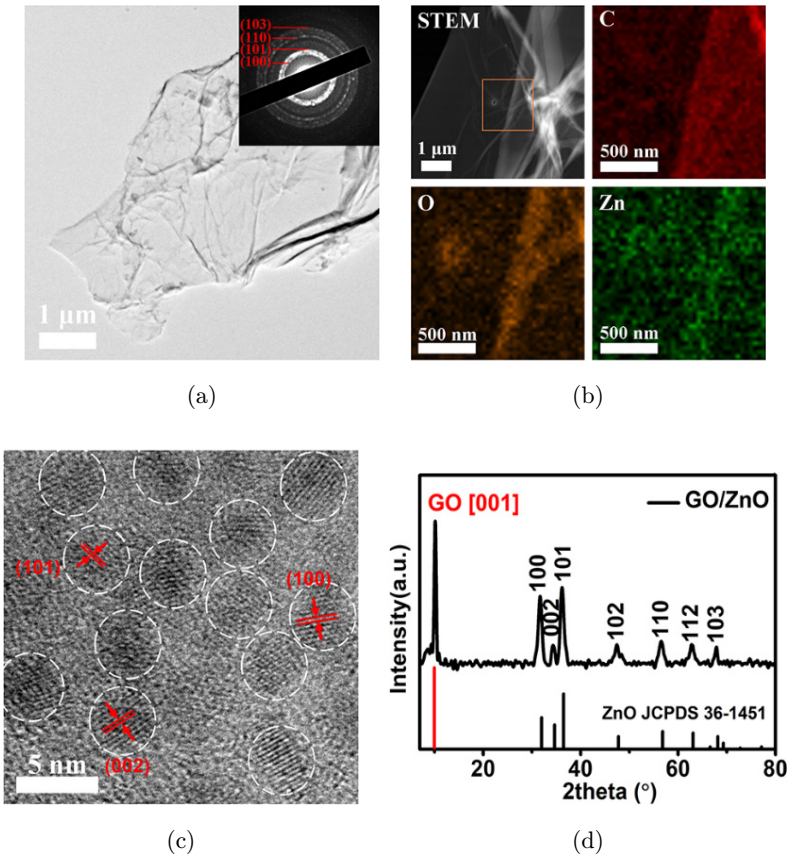

Fig. 3. (a) TEM micrograph and (inset) selected area electron diffraction (SAED) pattern of 2D GO/ZnO. (b) An EDS elemental map of 2D GO/ZnO includes an STEM micrograph (upper left) and elemental maps: C (upper right), O (lower left), and Zn (lower right). (c) HRTEM micrograph of the prepared 2D GO/ZnO. (d) Powder XRD diffractogram of 2D GO/ZnO. The red peak corresponds to GO (Color online).

average size of 3.9 ± 0.3 nm uniformly deposited on the surface of GO with clear lattice fringe spacings of 0.28 nm, 0.26 nm, and 0.25 nm corresponding to the (100), (002) and (101) crystal planes of ZnO, respectively.[35,36] The XRD diffractogram of our GO/ZnO nanosheets, shown in Fig. 3(d), contains a sharp reflection peak around 10°, corresponding to the (001) plane of GO. The remaining diffraction peaks are consistent with the lattice parameters of the Wurtzite phase structure of ZnO (JCPDS 36-1451). The SAED pattern in Fig. 3(a) also confirms the existence of polycrystalline ZnO nanoparticles with diffraction rings corresponding to the (100), (101), (110) and (103) planes of the standard Wurtzite phase ZnO, consistent with the XRD data.

The interaction between ZnO nanoparticles and GO was further investigated. Figure 4(a) shows FT-IR spectra of the three stages in the growth of GO/ZnO: GO, GO$-Zn^{2+}$ intermediates, and GO/ZnO nanocomposites. Several major absorption bands correspond to the oxygen-containing functional groups of GO. Characteristic bands at 3420, 1740, 1620, 1374, 1250 and 1060 cm^{-1} indicated the presence of O–H, carboxyl/carbonyl C=O, aromatic ring C=C, carboxyl C–O, epoxide/ether C–O, and alkoxy C–O bonds in GO, respectively.[37–39] In contrast, absorption peaks corresponding to carboxyl/carbonyl C=O and epoxide C–O bonds in GO$-Zn^{2+}$ intermediates and GO/ZnO nanocomposites were nearly invisible, while bands corresponding to alkoxy C–O bonds were shifted to lower wavenumbers. These phenomena show that coordination of carboxylic acid groups, ring-opened epoxides, and zinc played an important role in both the formation of intermediates and the uniform dispersion of ZnO nanoparticles.[40] Raman spectra of both GO and GO$-Zn^{2+}$ intermediates contained two characteristic peaks: a D band at 1300–1350 cm^{-1} and a G band at 1580–1620 cm^{-1} [Fig. 4(b)].[41,42]

The D band arises from the structural disorder of carbon atoms in the graphitic structure of layer

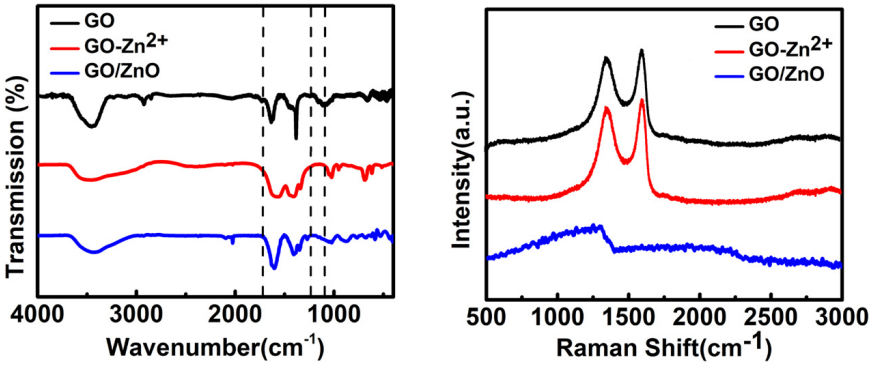

(a) (b)

Fig. 4. (a) FT-IR and (b) Raman spectra of GO, GO−Zn^{2+} and GO/ZnO.

edges, while the G band arises from the first-order scattering associated with the E_{2g} vibrational mode. Both bands are characteristic of carbon atoms in sp^2-hybridized states.[43] The relative intensity between the D and G bands (I_D/I_G) is an important parameter for identifying the relative number of structural defects in graphene. GO and GO−Zn^{2+} intermediates exhibited similar Raman spectra with I_D/I_G ratios less than 1 (0.93 for GO and 0.95 for GO−Zn^{2+} intermediates), indicating a similar degree of oxidation-induced lattice distortion between these two stages. Note that the anchoring of zinc cations did not change the structure of GO. However, both the D and G peaks were absent from the Raman spectrum of GO/ZnO, which might ascribe to high density loading of ZnO nanoparticles.[40,44]

The X-ray photoelectron spectroscopy (XPS) of GO and GO/ZnO has been shown in Fig. 5.

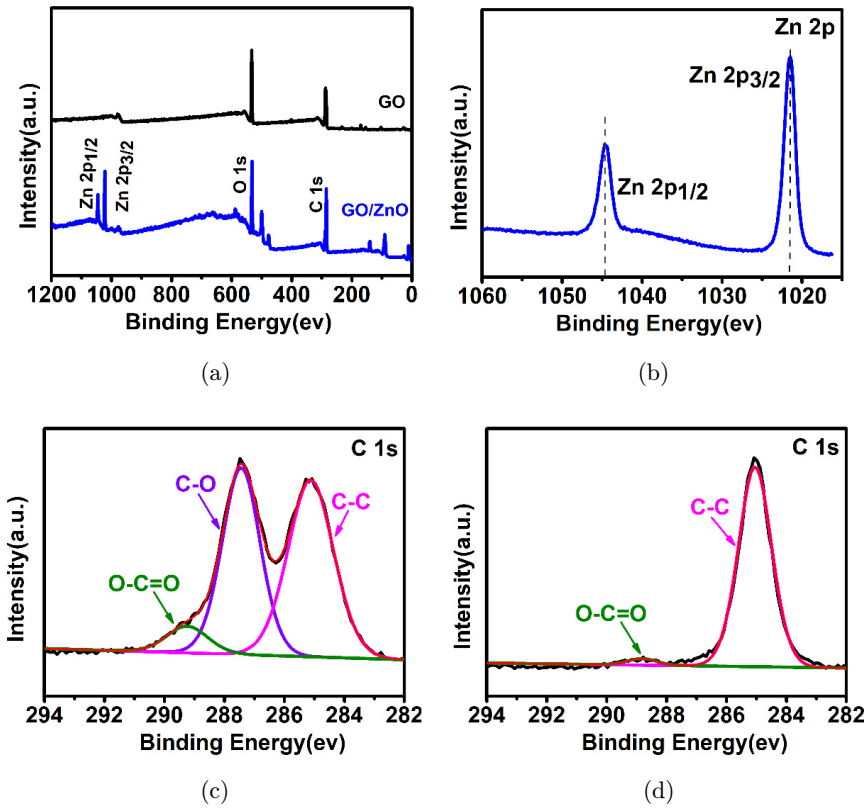

(a) (b) (c) (d)

Fig. 5. (a) XPS of GO and GO/ZnO; High-resolution XPS spectra of (b) Zn (2p), (c) C (1s) for GO and (d) C (1s) for GO/ZnO, respectively.

As shown in Fig. 5(a), peaks corresponding to C, O and Zn appeared in the GO/ZnO spectrum, while no Zn peak was observed in the GO. The data of GO for the C1s spectrum show C–C peak (285.0 eV), epoxy peak (C–O, 287.4 eV) and carboxyl (O–C=O, 289.3 eV) peaks [Fig. 5(c)].[45–47] In contrast, the C1s XPS spectrum for GO/ZnO [Fig. 5(d)] shows a completely disappeared component of the C–O, supporting that Zn^{2+} has led to the ring-opening reaction of epoxides.[48] Simultaneously, the O–C=O groups were shifted from 289.3 eV to 288.9 eV and the intensity decreased significantly for GO/ZnO, indicating the coordination between carboxylic acid and zinc. A detailed scan of the Zn region [Fig. 5(b)] contained a dual peak of the Zn $2p_{1/2}$ (1044.7 eV) and Zn $2p_{3/2}$ (1021.5 eV) certify that the oxidation state for zinc in GO/ZnO is Zn^{2+}.[49,50]

A dynamic equilibrium between adsorption and desorption exists in all mixtures of molecules and sorbent materials. This behavior is generally not conducive to high-performance desulfurization. With 2D sorbents, the adsorbed molecules are located only on the surface and steric hindrance does not limit molecular desorption. To overcome this phenomenon, our GO/ZnO nanosheets were further assembled into 3D porous scaffolds by thermal treatment. The porous structure effectively "traps" adsorbed sulfides and applies a spatial constraint on desorption, thereby increasing desulfurization activity. The SEM micrograph in Fig. 6(a) shows that a 3D GO/ZnO porous scaffold was successfully prepared with an average pore diameter of 283 ± 71 nm. The surface area of the scaffold was calculated using a Brunauer–Emmett–Teller (BET) adsorption isotherm model with nitrogen gas, yielding class IV isotherms [Fig. 6(b)]. The 3D scaffolds possessed a total surface area of 129 $m^2\,g^{-1}$ with a pore volume of 0.354 $cm^3\,g^{-1}$. The elemental content of these scaffolds was determined by EDS, which indicated 6.2 atom% Zn, 16.1 atom% O and 77.7 atom% C [Fig. 6(c)].

3.2. *Desulfurization performance*

The sulfur-containing substances in crude oil are generally classified as active sulfur or inactive sulfur. Thiophene and BT are typical inactive sulfides containing aromatic heterocyclic rings that are too chemically stable to be removed by current hydrodesulfurization technologies. To demonstrate the desulfurization performance of our 3D GO/ZnO scaffolds, four common sulfides (mercaptan, thioether, thiophene, BT), including both active and inactive sulfur moieties, were used. The most representative molecules in each group (ethanethiol, diethyl sulfide, thiophene, BT) were diluted with octane to formulate different model fuels, as listed in Table 1. To simulate the desulfurization realistically, real fluid catalytic cracking (FCC) gasoline was also evaluated. All adsorption experiments were carried out in a micro-high pressure reactor with an adsorbent/model fuel (or FCC gasoline) ratio of 15 mg/5 mL. The desulfurization process is illustrated in Fig. 7. Table 1 shows that single-component GO was not conducive to the removal of sulfides; the desulfurization rate was 12.02% for mercaptan, 14.01% for thioether, 17.01% for thiophene, 13.00% for BT and 10.02% for FCC gasoline. The weak desulfurization ability of GO was attributed to weak interactions, e.g., electrostatic, van der Waals and π–π stacking, between GO and sulfides. These were insufficient for tightly anchoring the

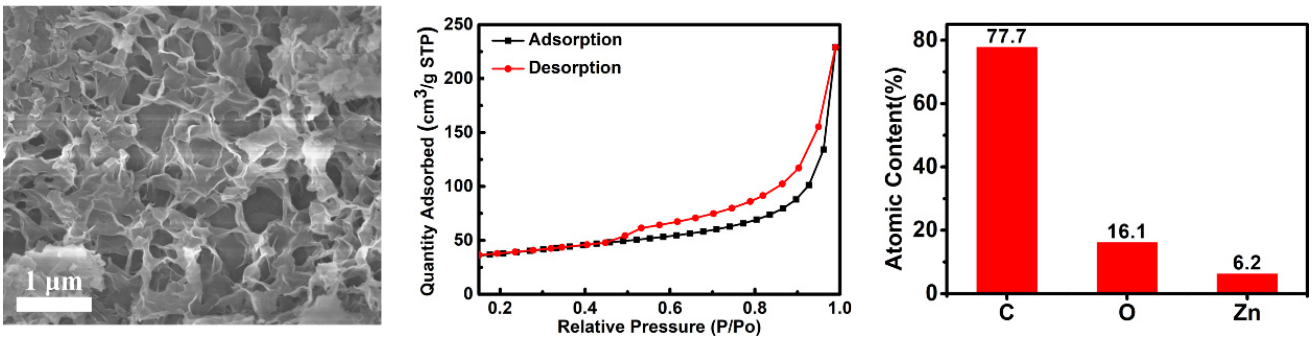

(a) (b) (c)

Fig. 6. (a) Representative SEM micrograph of 3D GO/ZnO. (b) N_2 adsorption/desorption isotherm of 3D GO/ZnO. (c) The elemental composition of 3D GO/ZnO scaffolds was determined by EDS.

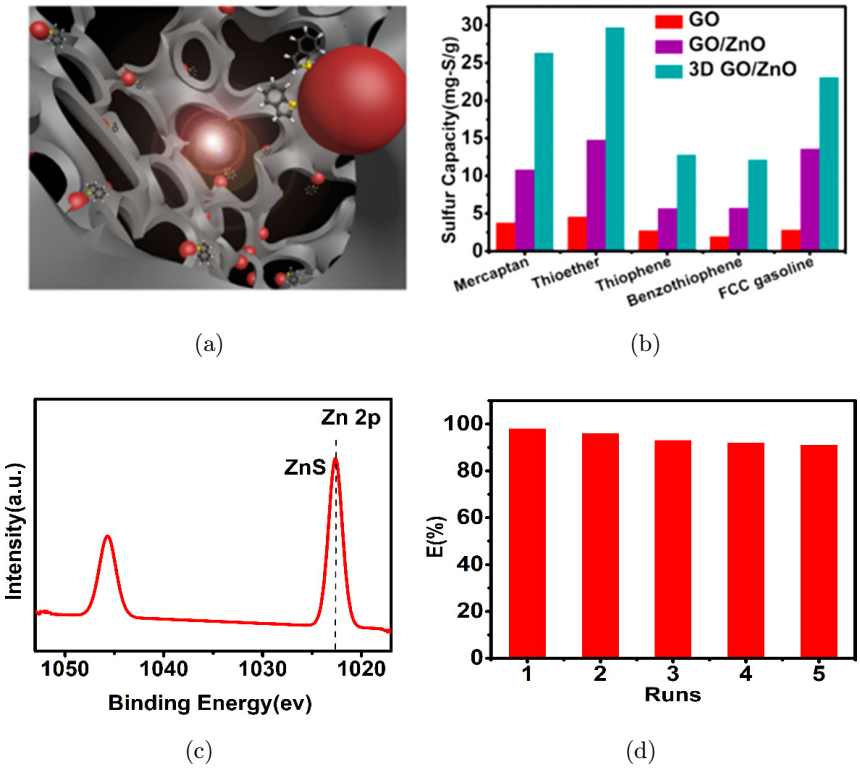

Fig. 7. (a) Schematic diagram of the removal of sulfides with a 3D GO/ZnO porous scaffold. (b) The sulfur adsorption capacities of GO, GO/ZnO and 3D GO/ZnO nanocomposites are shown for a variety of model fuels. (c) High-resolution XPS spectra of Zn (2p) for 3D GO/ZnO after desulfurization. (d) Regeneration capability of 3D GO/ZnO nanocomposites with thermal treatment.

Table 1. Desulfurization rates of GO, GO/ZnO and 3D GO/ZnO with different model fuels.

No.	Sample	Chemical formula	Initial sulfur content (ppm[a])	Sulfur content after desulfurization (ppm[b])			Sulfides removal (%)		
				GO	GO/ZnO	3D GO/ZnO	GO	GO/ZnO	3D GO/ZnO
1	Mercaptan	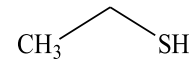	208.8	183.7	137.0	33.9	12.02	34.39	83.76
2	Thioether	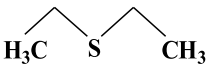	215.5	185.3	117.2	18.1	14.01	45.61	91.60
3	Thiophene	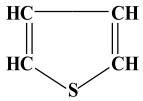	106.4	88.3	68.6	21.2	17.01	35.53	80.08
4	Benzothiophene	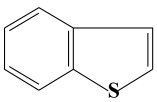	100.8	87.7	62.6	20.1	13.00	37.90	80.06
5	FCC gasoline	—	187.6	168.8	97.5	34.4	10.02	48.03	81.66

[a]The sulfur content of the model fuel.
[b]The sulfur content of the model fuel after desulfurization.

sulfide compounds. In contrast, uniform growth of ZnO nanoparticles on the surface of GO significantly enhanced the specific binding of sulfides, resulting in a removal efficiency of 34.39% for mercaptan, 45.61% for thioether, 35.53% for thiophene, 37.90% for BT and 48.03% for FCC gasoline.

The 3D GO/ZnO scaffolds exhibited the strongest adsorption capacity. The sulfide removal

efficiency of 3D GO/ZnO scaffolds (83.76% for mercaptan, 91.60% for thioether, 80.08% for thiophene, 80.06% for BT and 81.66% for FCC gasoline) was 5–7 times higher than that of GO, and about twice that of GO/ZnO. Sulfur adsorption capacities were also calculated; the 3D GO/ZnO scaffolds had the highest adsorption capacity regardless of the chemical nature of the sulfide, reaching a highest value of 29.73 mg S/g adsorbent for the removal of thioethers. These results provide clear evidence that uniform dispersion of nanosorbents on suitable carriers, and the construction of 3D porous structures, are effective means of increasing adsorption activity.

To interaction between 3D GO/ZnO scaffold and sulfides was further evaluated by XPS. As illustrated in Fig. 7(c), the higher binding energy component of Zn (2p) at 1022.6 eV was attributed to the formation of Zn–S bond.[51] This result confirmed that the well-dispersed ZnO nanoparticles on the surface of GO could bind sulfides specifically, achieving excellent desulfurization performance. Apart from the adsorption properties, the recycling ability of GO/ZnO scaffold is another important indicator in industrial applications. The 3D GO/ZnO adsorbents could be easily regenerated by simple thermal treatment approach. In the fifth cycle, the 3D GO/ZnO scaffolds could still keep 91% of the initial desulfurization efficiency [Fig. 7(d)].

The mechanism underlying the excellent desulfurization performance of 3D GO/ZnO scaffolds could be attributed to the following points: (i) the super-dispersed ZnO nanoparticles grown on the surface of graphene, processing high chemisorption capacity, could combine with sulfides through Zn–S bonds; (ii) graphene oxide could synergistically adsorb aryl sulfides via π–π stacking interactions; (iii) the self-assembled 3D porous structure can effectively trap sulfides and inhibited desorption.

4. Conclusions

Three-dimensional GO/ZnO porous scaffolds were synthesized for the efficient desulfurization of transportation fuels. The GO/ZnO nanocomposites facilitated specific adsorption of sulfides, and the self-assembly of porous, 3D GO/ZnO scaffolds further increased desulfurization rates by effectively "trapping" sulfide compounds. The adsorption capacity of our 3D GO/ZnO scaffold was 5–7- and $\sim$ 2-fold higher than those of GO and 2D GO/ZnO, respectively. The highest sulfur adsorption capacity of our 3D GO/ZnO scaffold was 29.73 mg S/g adsorbent. This study introduces a novel strategy for fabricating 3D GO-based nanocomposites and demonstrates the potential of these materials for future catalytic applications.

Acknowledgments

Yan Liu, Xiaojun Zhang, Meiyan Yang contributed equally. This research was financially supported by the Beijing Municipal Natural Science Foundation No. 2184119 (D. L.), the Science Foundation of China University of Petroleum, Beijing No. 2462018BJB002 (D. L.), Projects of Beijing Nova Programme Interdisciplinary Cooperation Project No. Z181100006218135 (Y. L. and D. L.), National Natural Science Foundations of China No. 81571815 (Y. L.), No. 81871492 (Y. L.) and No. 51902344 (D. L.).

References

1. Y. Nath Prajapati and N. Verma, *Energy Fuels* **32**, 2183 (2018), doi: 10.1021/acs.energyfuels.
2. G. I. Danmaliki and T. A. Saleh, *Chem. Eng. J.* **307**, 914 (2017), doi: 10.1016/j.cej.2016.08.143.
3. J. Fujiki and E. Furuya, *Fuel* **164**, 180 (2016), doi: 10.1016/j.fuel.2015.10.013.
4. T. A. Saleh, K. O. Sulaiman, S. A. Al-Hammadi, H. Dafalla and G. I. Danmaliki, *J. Clean. Prod.* **154**, 401 (2017), doi: 10.1016/j.jclepro.2017.03.169.
5. M. T. Timko, J. A. Wang, J. Burgess, P. Kracke, L. Gonzalez and C. Jaye, *Fuel* **163**, 223 (2016), doi: 10.1016/j.fuel.2015.09.075.
6. H. Zhang, Q. Zhang, L. Zhang, T. Pei, L. Dong, P. Zhou and L. Xia, *Chem. Eng. J.* **334**, 285 (2018), doi: 10.1016/j.cej.2017.10.042.
7. V. C. Srivastava, *RSC Adv.* **2**, 759 (2012), doi: 10.1039/C1RA00309G.
8. M. Hayyan, M. H. Ibrahim, A. Hayyan, I. M. Alnashef, A. M. Alakrach and M. A. Hashim, *Ind. Eng. Chem. Res.* **54**, 12263 (2015), doi: 10.1021/acs.iecr.5b03427.
9. B. Jiang, H. Yang, L. Zhang, R. Zhang, Y. Sun and Y. Huang, *Chem. Eng. J.* **283**, 89 (2016), doi: 10.1016/j.cej.2015.07.070.
10. M. Ibrahim, H. M. Hayyan, M. A. Hashim and A. Hayyan, *Renew. Sust. Energ. Rev.* **76**, 1534 (2017), doi: 10.1016/j.rser.2016.11.194.
11. R. Abro, A. A. Abdeltawab, S. S. Al-Deyab, G. Yu, A. B. Qazi and S. Gao, *RSC Adv.* **4**, 35302 (2014), doi: 10.1039/C4RA03478C.
12. T. C. Chen, Y. H. Shen, W. J. Lee, C. C. Lin and M. W. Wan, *J. Clean. Prod.* **39**, 129 (2013), doi: 10.1016/j.jclepro.2012.09.001.

13. F. S. Mjalli, O. U. Ahmed, T. Al-Wahaibi, Y. Al-Wahaibi and I. M. AlNashef, *Rev. Chem. Eng.* **30**, 337 (2014), doi: 10.1515/revce-2014-0001.
14. P. S. Kulkarni and C. A. M. Afonso, *Green Chem.* **12**, 1139 (2010), doi: 10.1039/c002113j.
15. S. Luo, J. Liu and Z. Wu, *J. Phys. Chem. C.* **123**, 11772 (2019), doi: 10.1021/acs.jpcc.9b02155.
16. M. T. Baei, M. B. Tabar and S. Hashemian, *Adsorpt. Sci. Technol.* **31**, 469 (2013), doi: 10.1260/0263-6174.31.5.469.
17. L. Huang, G. Wang, Z. Qin, M. Dong, M. Du, H. Ge and J. Wang, *Appl. Catal., B* **106**, 26 (2011), doi: 10.1016/j.apcatb.2011.05.001.
18. C. L. Carnes and K. J. Klabunde, *Langmuir* **16**, 3764 (2000), doi: 10.1021/la991498p.
19. E. Sasaoka, S. Hirano, S. Kasaoka and Y. Sakata, *Energy Fuels* **8**, 763 (1994), doi: 10.1021/ef00045a033.
20. C. Yang, J. Kou, H. L. Fan, Z. Tian, W. Kong and J. Shangguan, *Langmuir* **35**, 7759 (2019), doi: 10.1021/acs.langmuir.9b00853.
21. X. Meng, H. Huang and L. Shi, *Ind. Eng. Chem. Res.* **52**, 6092 (2013), doi: 10.1021/ie303514y.
22. K. S. Novoselov, A. K. Geim, S. V. Morozov, D. Jiang, Y. Zhang, S. V. Dubonos and A. A. Firsov, *Science* **306**, 666 (2004), doi: 10.1126/science.1102896.
23. K. S. Kim, Y. Zhao, H. Jang, S. Y. Lee, J. M. Kim, K. S. Kim and B. H. Hong, *Nature* **457**, 706 (2009), doi: 10.1038/nature07719.
24. C. Zhu, S. Guo, Y. Fang and S. Dong, *ACS Nano* **4**, 2429 (2010), doi: 10.1021/nn1002387.
25. M. Sun, H. Liu, Y. Liu, J. Qu and J. Li, *Nanoscale* **7**, 1250 (2015), doi: 10.1039/c4nr05838k.
26. M. Seredych, O. Mabayoje and T. J. Bandosz, *Langmuir* **28**, 1337 (2012), doi: org/10.1021/la204277c.
27. A. J. Hernandez-Maldonado and R. T. Yang, *Ind. Eng. Chem. Res.* **43**, 1081 (2004), doi: 10.1021/ie034206v.
28. D. C. Marcano, D. V. Kosynkin, J. M. Berlin, A. Sinitskii, Z. Sun, A. Slesarev *et al. ACS NANO* **4**, 4806 (2010), doi: 10.1021/nn1006368.
29. J. H. Kang, T. Kim, J. Choi, J. Park, Y. S. Kim, M. S. Chang *et al. Chem. Mater.* **28**, 756 (2016), doi: 10.1021/acs.chemmater.5b03700.
30. M. D. P. Lavin-Lopez, A. Romero, J. Garrido, L. Sanchez-Silva and J. L. Valverde, *Ind. Eng. Chem. Res.* **55**, 12836 (2016), doi: 10.1021/acs.iecr.6b03533.
31. K. Wu, K. Du and G. Hu, *J. Mater. Chem. A* **6**, 3444 (2018), doi: 10.1039/C7TA10850H.
32. L. Wang, R. T. Yang and C. L. Sun, *AlChE J.* **59**, 29 (2013), doi: 10.1002/aic.13896.
33. P. Ramesh, S. Bhagyalakshmi and S. Sampath, *J. Colloid Interface Sci.* **274**, 95 (2004), doi: 10.1016/j.jcis.2003.11.030.
34. S. Peng, X. Fan, S. Li and J. Zhang, *J. Chil. Chem. Soc.* **58**, 2213 (2013), doi: 10.4067/S0717-97072013000400067.
35. E. Y. Salih, M. F. M. Sabri, K. Sulaiman, M. Z. Hussein, S. M. Said, R. Usop and M. B. A. Bashir, *Mater. Res. Express* **5**, 116202 (2018), doi: 10.1088/2053-1591/aadbca/meta.
36. J. A. Barón-Miranda, O. Calzadilla, S. San-Juan-Hernández, I. Diez-Pérez, J. Díaz, F. Sanz and F. Caballero-Briones, *J. Mater. Sci. -Mater. Electron.* **29**, 2016 (2018), doi: 10.1007/s10854-017-8113-x.
37. W. Chen and L. Yan, *Nanoscale* **2**(4), 559 (2010), doi: 10.1039/B9NR00191C.
38. E. Y. Choi, T. H. Han, J. Hong, J. E. Kim, S. H. Lee, H. W. Kim and S. O. Kim, *J. Mater. Chem.* **20**, 1907 (2010), doi: 10.1039/B919074K.
39. G. Gollavelli and Y. C. Ling, *Biomaterials* **33**, 2532 (2012), doi: 10.1016/j.biomaterials.2011.12.010.
40. Y. T. Liu, M. Dang, X. M. Xie, Z. F. Wang and X. Y. Ye, *J. Mater. Chem.* **21**, 18723 (2011), doi: 10.1039/C1JM13727A.
41. Y. Qi, *J. Mater. Res.* **33**, 1560 (2018), doi: org/10.1557/jmr.2018.110.
42. S. A. Hosseini and S. Babaei, *J. Braz. Chem. Soc.* **28**, 299 (2017), doi: 10.5935/0103-5053.20160176.
43. A. C. Ferrari and J. Robertson, *Phys. Rev. B* **61**, 14095 (2000), doi: 10.1103/PhysRevB.61.14095.
44. J. Hwang, T. Yoon, S. H. Jin, J. Lee, T. S. Kim, S. H. Hong *et al. Adv. Mater.* **25**, 6724 (2013), doi: 10.1002/adma.201302495.
45. S. Pei, Q. Wei, K. Huang, H. M. Cheng and W. Ren, *Nat. Commun.* **9**, 145 (2018), doi: 10.1038/s41467-017-02479-z.
46. H. W. Kim, M. B. Ross and N. Kornienko, *Nat. Catal.* **1**, 282 (2018), doi: 10.1038/s41929-018-0044-2.
47. S. Panda, T. K. Rout, A. D. Prusty, P. M. Ajayan and S. Nayak, *Adv. Mater.* **30**, 1702149 (2018), doi: 10.1002/adma.201702149.
48. Y. Li, X. Liu, X. Chen, D. Wang and Y. He, *J. Alloy. Compd.* **12**, 364 (2017), doi: 10.1016/j.jallcom.2016.12.364.
49. H. S. Song, M. G. Park, S. J. Kwon, K. B. Yi, E. Croiset, Z. Chen and S. C. Nam, *Appl. Surf. Sci.* **276**, 646 (2013), doi: 10.1016/j.apsusc.2013.03.147.
50. O. Akhavan, *Carbon* **49**, 11 (2011), doi: 10.1016/j.carbon.2010.08.030.
51. R. Inoue, M. Kitagawa, T. Nishigaki *et al. Appl. Surf. Sci.* **142**, 341 (1999), doi: org/10.1016/S0169-4332(98)00672-2.